Editor's note: A Correction was published on 8th February 2021 that affects Table S4 of this ESI. This Correction can be viewed online at https://doi.org/10.1039/D1TA90025K

Activating the Lattice Oxygen in $(Bi_{0.5}Co_{0.5})_2O_3$ by Vacancy Modulation for Efficient Electrochemical Water Oxidation

Huan Liu,[1] Xiaoning Li,[2] Cailing Peng,[1] Liuyang Zhu,[1] Yuanxi Zhang,[1] Huiru Cheng,[3] Jiameng Cui,[1] Qingmei Wu,[1] Yingying Zhang,[1] Zezhi Chen,[1] Wei Zou,[1] Wen Gu,[1] Haoliang Huang,[2,4] Jianlin Wang,[2,4] Bangjiao Ye,[3] Zhengping Fu*,[1,2,4] and Yalin Lu*,[1,2,4]

[1]*Department of Materials Science and Engineering, CAS Key Laboratory of Materials for Energy Degradation, University of Science and Technology of China, Hefei 230026, P. R. China*

[2]*Synergetic Innovation Center of Quantum Information and Quantum Physics & Hefei National Laboratory for Physical Sciences at Microscale, University of Science and Technology of China, Hefei 230026, P. R. China*

[3]*State Key Laboratory of Particle Detection and Electronics, University of Science and Technology of China, Hefei 230026, P. China*

[4]*Anhui Laboratory of Advanced Photon Science and Technology, University of Science and Technology of China, Hefei 230026, P. R. China*

**Corresponding authors. E-mail: fuzp@ustc.edu.cn; yllu@ustc.edu.cn.*

Experiment Section

Synthesis of Sheet-like BCO with Oxygen-vacancy Defects: All chemical reagents were analytic grade without further purifying. Co doped Bi_2O_3 (named as BCO) with oxygen vacancies were synthesized via coprecipitation method and subsequent heat treatment. In a typical process, 2 *m*mol $Bi(NO_3)_3 \cdot 5H_2O$ and 2 *m*mol $Co(NO_3)_2 \cdot 6H_2O$ were added and dissolved in 5 *m*l nitric acid (4M) and 10 *m*l deionized water, respectively, and then were mixed. Subsequently, 1.375 g sodium hydroxide was dissolved in 50 *m*l H_2O and then was dropped into the mixed solution and continuously stirred for 1 h and aged for overnight. The obtained precursor was washed with deionized water several times and then was dried in an oven at 60 ℃ overnight. After calcination at 400 ℃ for 2 h at the heating rate of 5 ℃ min^{-1} under air or pure oxygen atmosphere, the oxygen-vacancy-rich and oxygen-vacancy-poor BCO were obtained respectively.

Structure Characterization: The morphologies of the as-prepared samples were characterized by scanning electron microscopy (SEM; JSM-6700F), transmission electron microscopy (TEM), high-resolution transmission electron microscopy (HRTEM; JEM-2010, 200KV) and mapping images. Crystal structures were recorded by X-ray diffraction (XRD, Rigaku-TTR III) with Cu Kα radiation (40 *k*V, 30 *m*A, 1.5406 Å). Element composition was analyzed using an ICP atomic emission spectrometer (Optima 7300 DV). The soft X-ray absorption spectra (XAS) were collected at the BL10B of the National Synchrotron Radiation Laboratory (NSRL,

Hefei, P. R. China). X-ray photoelectron spectroscopy (XPS) measurement was carried out using an ESCALAB 250 X-ray photoelectron spectrometer with Al-Kα irradiation. Ultraviolet-photoelectron spectroscopy (UPS) were acquired with an ESCALAB 250 X-ray photoelectron spectrometer using He I (i.e., 21.2 eV) ultraviolet radiation and the pass energy is 1.00 eV. The BET surface area was determined using N_2 sorption isotherm measurement (Tristar II 3020M). The element compositions of samples were observed by the electron probe microanalyzer (EPMA-8050G, Shimadzu). Positron annihilation spectra (PAS) were conducted with a fast-slow coincidence ORTEC system with a time resolution of about 230 *p*s, in which the samples were pressed into disks with about 1-*m*m thick, anda 5 *m*Ci source of ^{22}Na was sandwiched between two identical sample disks.

Computational methods and models: The spin-polarized density functional theory (DFT) with calculations of BCO and V_o-BCO (with oxygen vacancy) were performed by the Vienna ab initio simulation package (VASP). The Perdew-Burke-Ernzerhof (PBE) functional within generalized gradient approximation (GGA) for the exchange-correlation contribution has been employed. The cutoff energy of 400 eV is used for the plane-wave basis set. LDA+U with the Coulomb U value of 2.5 is considered for the 3*d* electrons in the cobalt element. Geometry optimization of BCO was performed at first, then V_o-BCO was obtained by enlarging the BCO cell to 2x1x2 supercell, followed by removing one oxygen atom in the supercell. The geometry optimization of V_o-BCO was performed accordingly. The k-point meshes of the Brillouin zone sampling for BCO and V_o-BCO was set at 1x2x1 and 2x2x3, based on the Monkhorst-

Pack scheme, respectively. The SCF tolerance of 1.0×10^{-6} eV/atom was taken as the electronic convergence criteria. The residual force was geometry-optimized to smaller than 0.01 eV/Å. For the density of states (DOS) calculation, the 2x1x2 supercell of BCO is used, and the k-point sampling of the Brillouin zone is 2x3x2 for BCO supercell and V_o-BCO. The energies of V_o-BCO with oxygen vacancy at different sites are compared, and the case shown in Figure S4 is with the lowest energy. Therefore, the following analysis is based on this situation. For the DOS comparison of BCO and V_o-BCO, only the atoms around the oxygen vacancy (indicated in Figure S4) is used for calculating PDOS.

Electrical Conductivity Measurement: The samples were firstly pressed into thin slices under 10 *M*Pa, the resistances (R) were measured using a Keithley model 2000 multimeter instrument. The electrical conductivities (σ) of the samples were calculated via $R=\rho L/S$ and $\sigma=1/\rho$, where ρ, L and S represent the electrical resistivity, length and cross-sectional area of the pressed sample, respectively.

Electrochemical Measurement: All the electrochemical measurements were conducted in a typical three-electrode system on an electrochemical workstation (CHI 660E, Chenhua, Shanghai) in 1.0 M KOH electrolyte solution, with platinum wires, saturated Ag/AgCl, and glassy carbon electrode with a diameter of 3 *m*m as the counter electrode, reference electrode, and working electrode, respectively. For work electrode preparation, 10 *m*g catalyst and 5 *m*g carbon black were suspended in 1 *m*l isopropanol-water solution (volume ratio = 3:1) with 0.1 *m*L of 5 wt% Nafion solution to form a homogeneous ink which was ultrasonicated for 1 h. Then 3 μL of the ink was spread

onto the surface of the glassy carbon electrode (mass loading: 0.386 mg·cm^{-2}) and dried under room temperature. Before the OER measurements, the electrolyte was purged with high-purity oxygen about 30 min. Linear sweep voltammetry (LSV) was collected with a scan rate of 5 mV·s^{-1} to minimize the capacitive current. The Tafel plots were obtained from the corresponding polarization curves. The Tafel slope (b) was obtained according to the Tafel equation ($\eta = b \log j + a$). (η is overpotential, j is anodic current density). The electrochemical impedance spectroscopy (EIS) was tested at 1.61 V (vs. RHE) in the frequency range from 10^5 to 0.1 Hz with an amplitude of 5 mV. The cycling stability curve was measured by a chronoamperometry at the overpotential of 410 mV (vs. RHE) for several hours. The electrochemical surface areas (ECSA) was determined by measuring the capacitive current associated with double-layer charging from the scan-rate dependence of cyclic voltammetry (CV). The potential window of CV was 1.01 - 1.11 vs. RHE. The scan rates were 2, 4, 6, 8, and 10 mV·s^{-1}. The double-layer capacitance (C_{dl}) was estimated by plotting the $\Delta J = (J_+ - J_-)/2$ at 1.06 V vs. RHE against the scan rate. The specific capacitance for a flat surface is generally found to be in the range of 20~60 μF·cm^{-2}.[1] The value of 60 μF·cm^{-2} was used in the following calculation of the ECSA.

Electrochemical Calculation: All the current density was normalized to the geometrical surface area and the potentials (as. Ag/AgCl) were corrected to the reversible hydrogen electrode (RHE) according to the equation (1):

$$E_{\mathrm{RHE}} = E_{\mathrm{Ag/AgCl}} + 0.059 \times \mathrm{pH} + 0.197 \quad (1)$$

In this work, E_{RHE} is corrected following the equation: E_{iR} corrected$=E_{\mathrm{RHE}} - iR_{\mathrm{s}}$

(where i is the current, and R_s is the uncompensated ohmic solution resistance resolved from Nyquist plots.)

The value of turnover frequency (TOF) were calculated by assuming that every Co atom is involved in the catalysis according to the equation (2):

$$TOF = \frac{j \times A}{4 \times F \times n} \tag{2}$$

where j (mA·cm^{-2}) is the measured current density at η = 380 mV, A is the geometry surface area of the glassy carbon electrode, the factor 4 means that 4 electrons are required to form one oxygen molecular, F is Faraday's constant (96485 C·mol^{-1}), and n is the moles of active sites on the electrode.

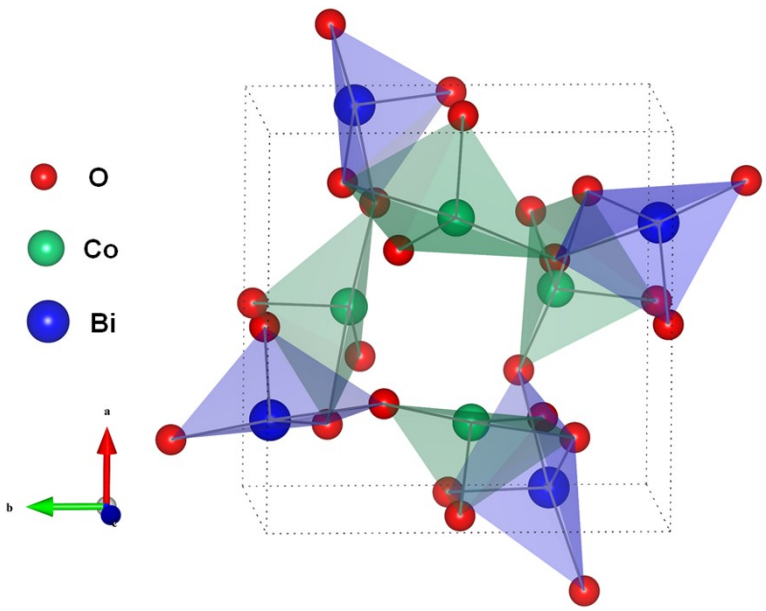

Figure S1. Crystal model of tetragonal BCO.

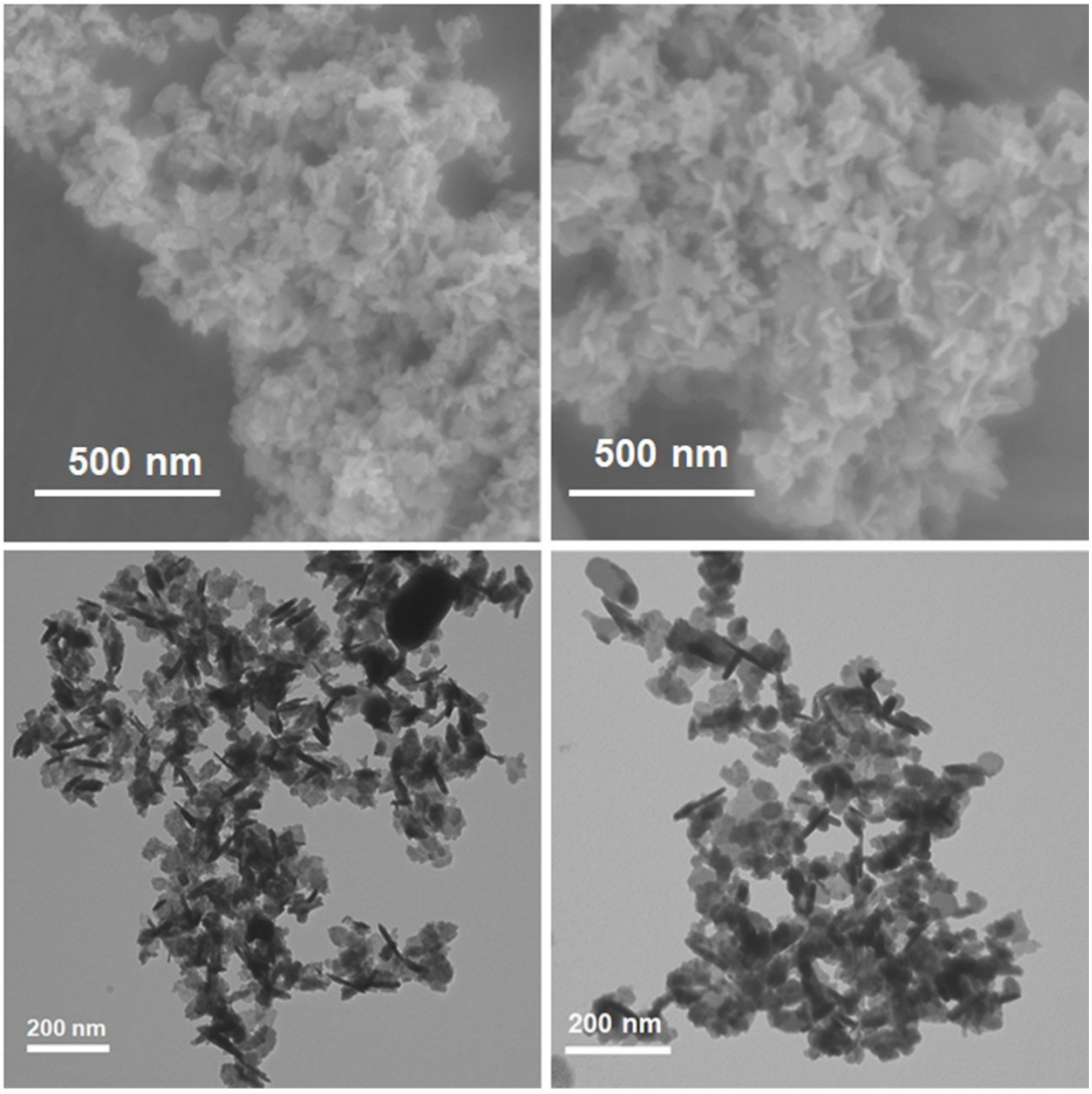

Figure S2. SEM images of a) V_o-rich BCO, and b) V_o-poor BCO. TEM images of c) V_o-rich BCO, and d) V_o-poor BCO.

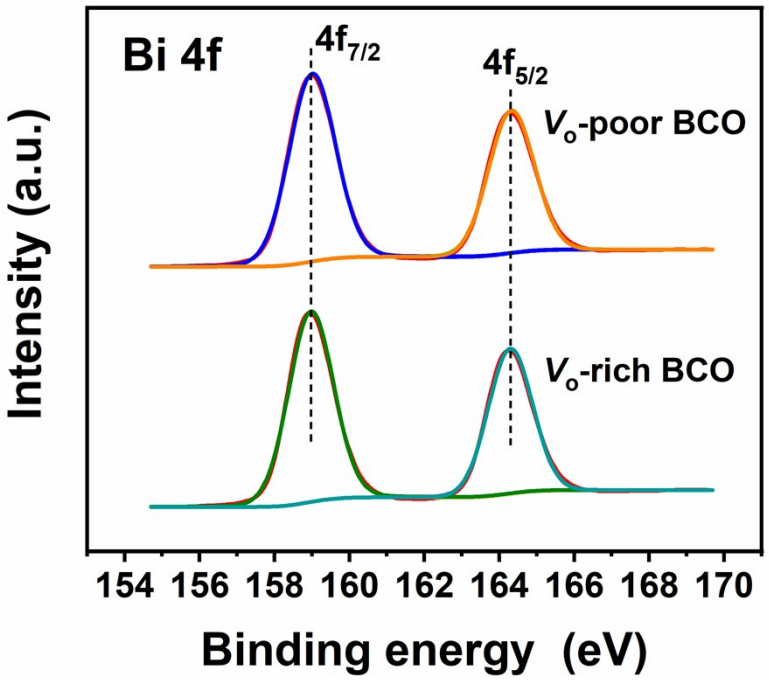

Figure S3. Bi 4*f* XPS spectra of the as-prepared catalysts.

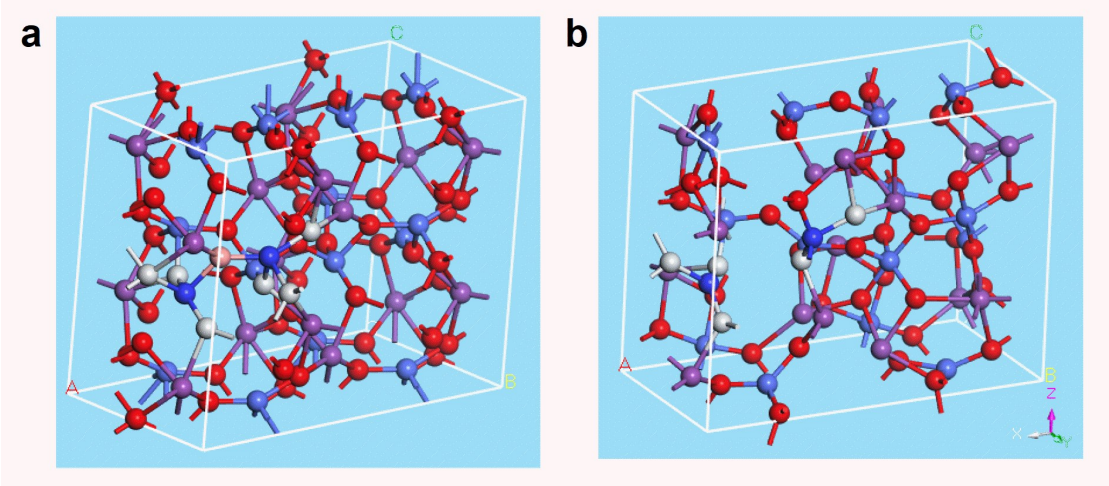

Figure S4. a) V_o-BCO model; b) BCO model. One oxygen atom in BCO was removed to get the V_o-BCO structure. The two Co atoms (Blue) around the oxygen vacancy (Pink) and the oxygen atoms (white) bonded to these two Co atoms are adopted to calculate the PDOS changement after the presence of oxygen vacancy.

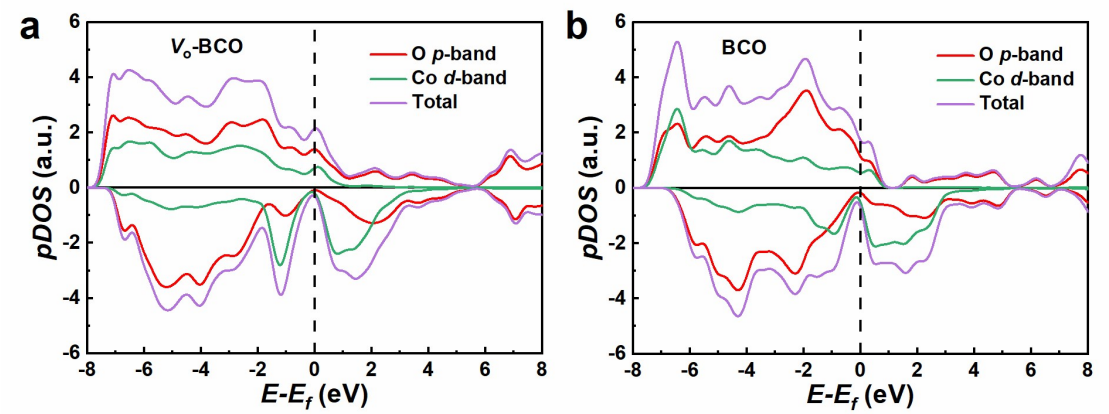

Figure S5. The computed PDOS of the Co atoms and the oxygen atoms indicated in Figure S4.

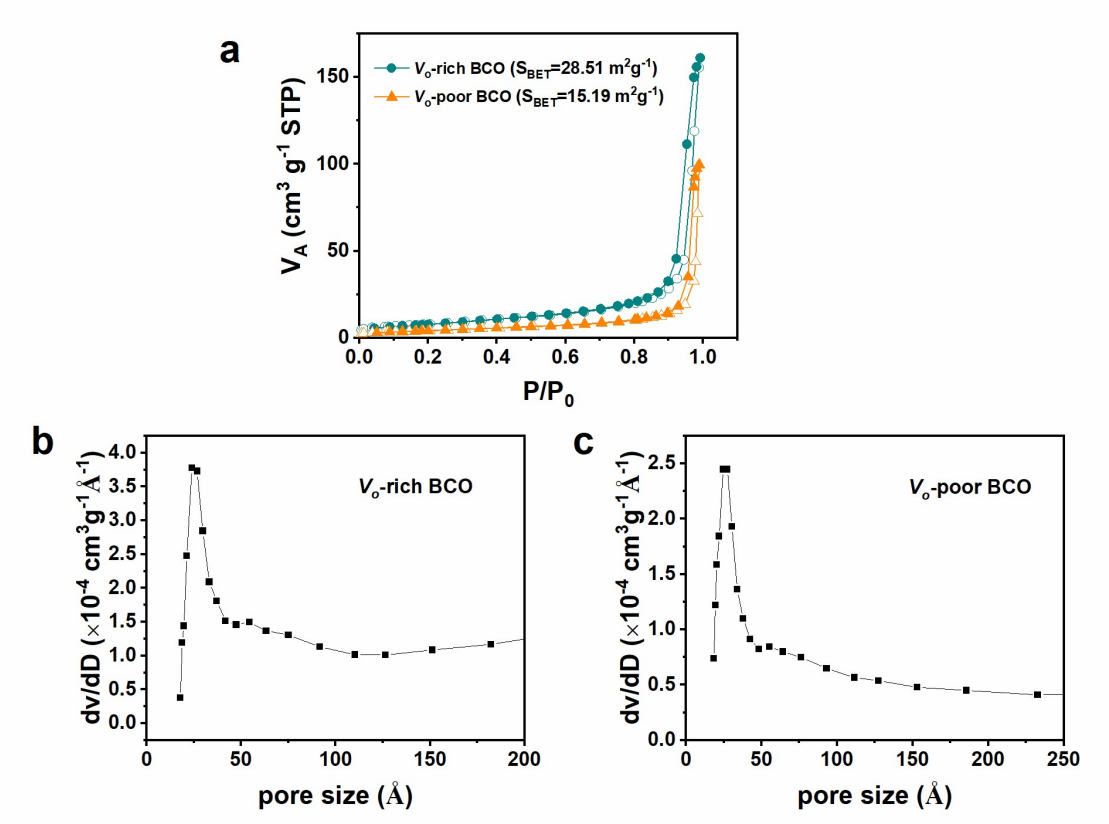

Figure S6. (a) Nitrogen adsorption-desorption isotherms. The pore structure of b) V_o-rich BCO, and c) of V_o-poor BCO.

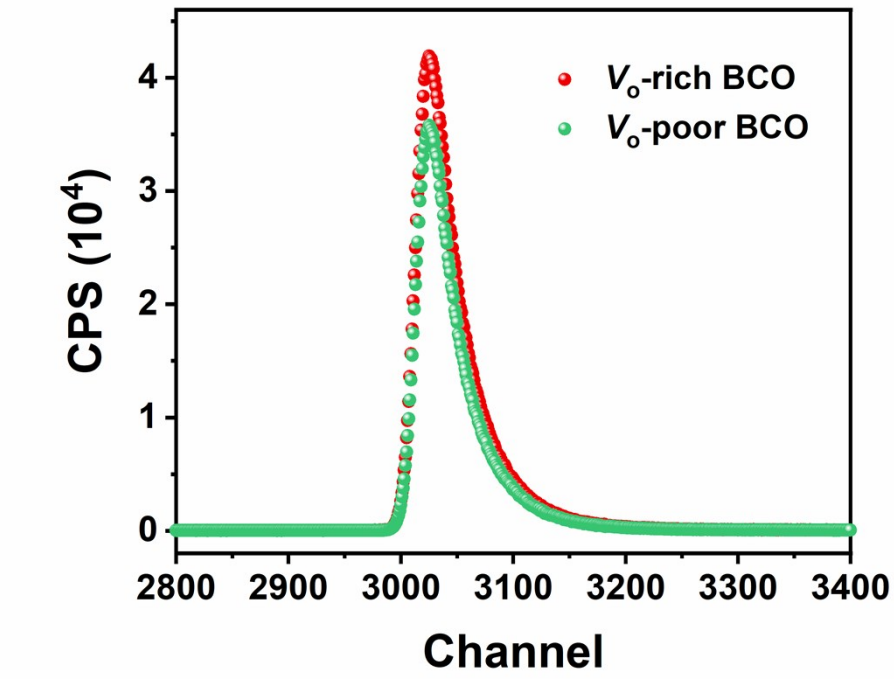

Figure S7. Positron annihilation spectra of the as-prepared catalysts.

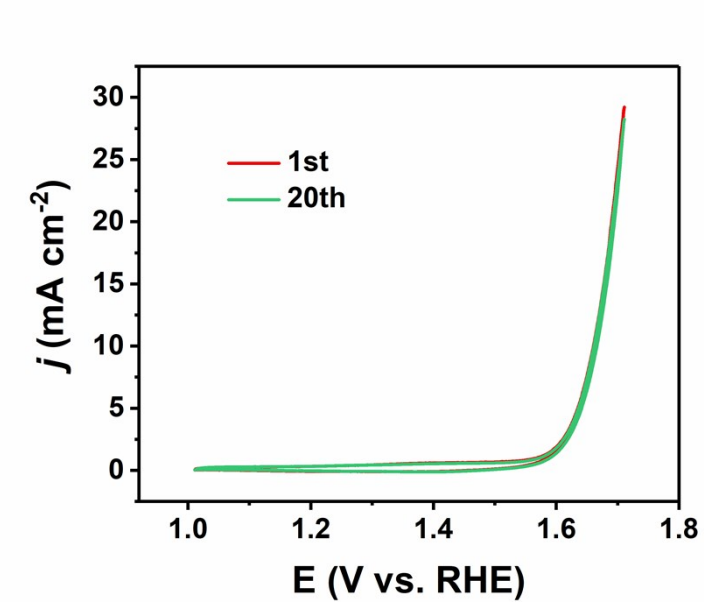

Figure S8. The OER CV curves without *iR*-correction of V_o-rich BCO in O_2-saturated 1.0 M KOH (scan rate: 5 mV·s^{-1}).

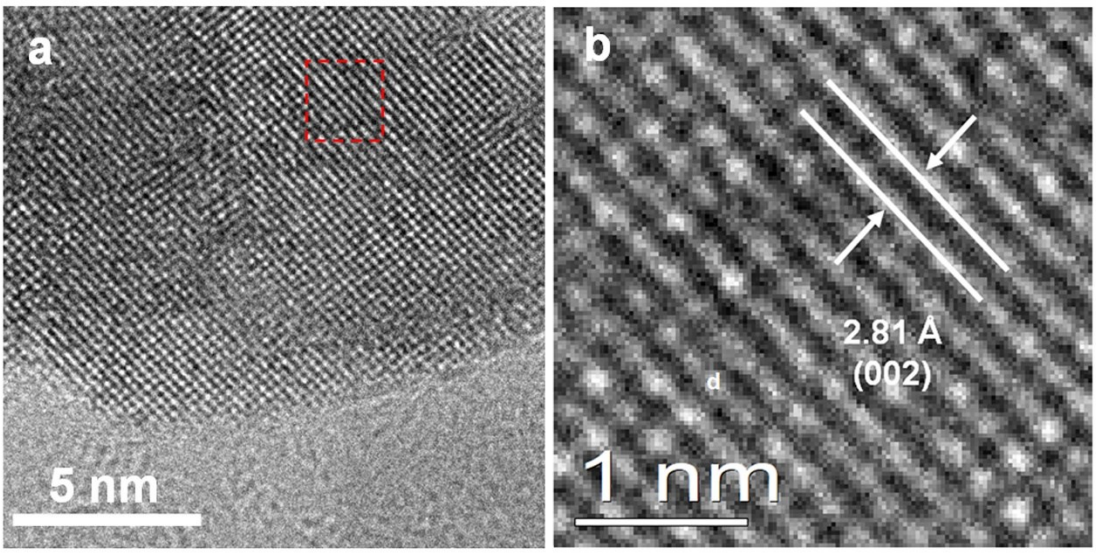

Figure S9. a) the high-resolution TEM image of V_o-rich BCO. b) the enlarge HRTEM image of rectangular area in red of left image.

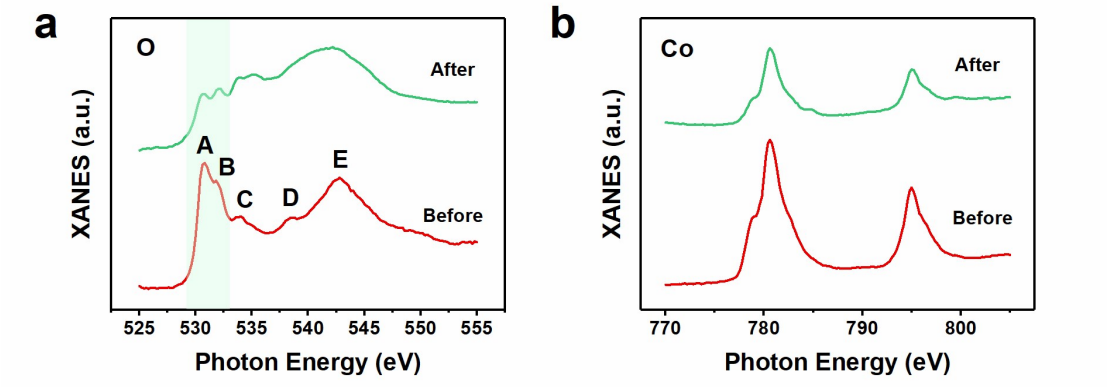

Figure S10. a) Normalized O *K*-edge and b) Normalized Co *L*-edge XAS spectra of V_o-rich BCO catalysts before and after the long-term test.

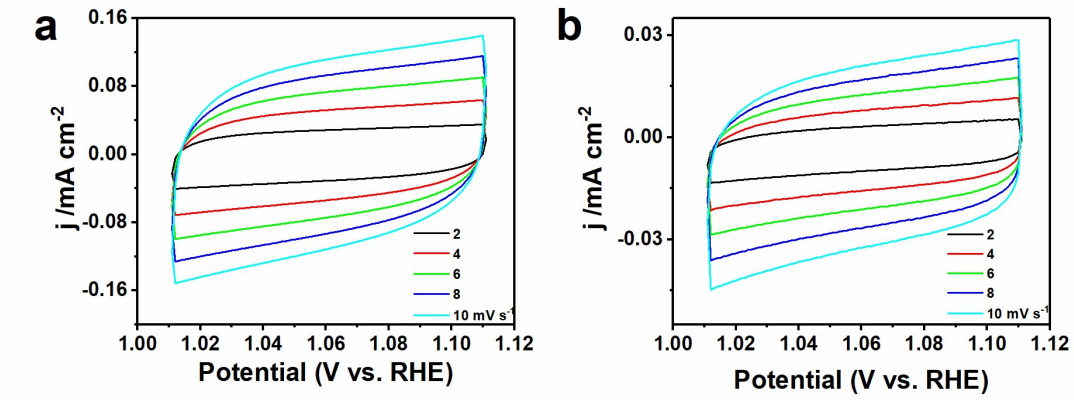

Figure S11. The electric double-layer capacitance measurements of V_o-rich BCO and V_o-poor BCO catalysts. ECSA of an electrocatalyst is proportional to C_{dl}, which can be evaluated by CV tests. Thus V_o-rich BCO shows a higher ECSA than that of V_o-poor BCO.

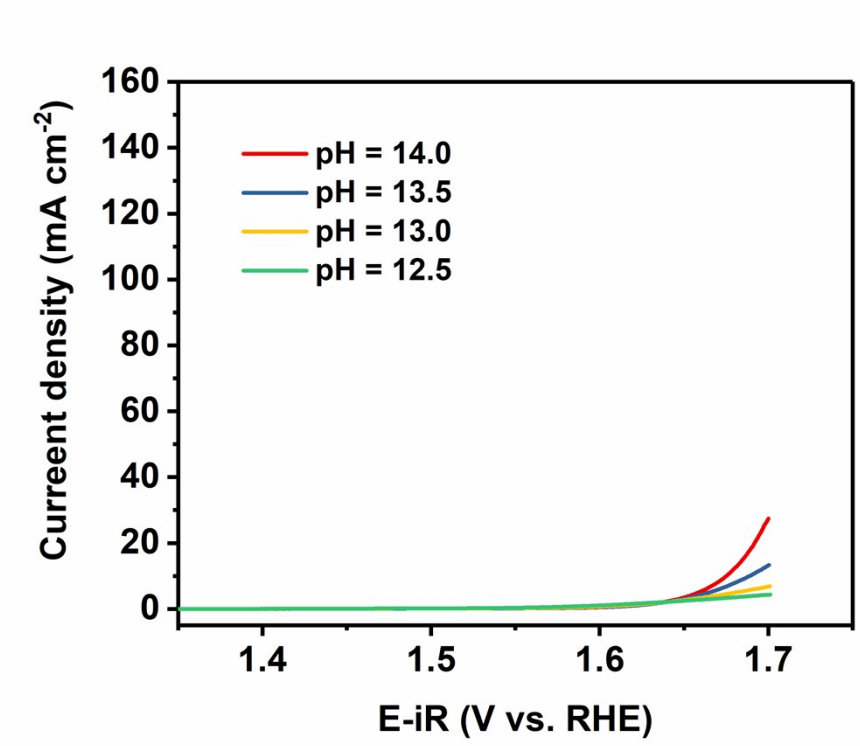

Figure S12. pH dependence of the OER activity of V_o-poor BCO.

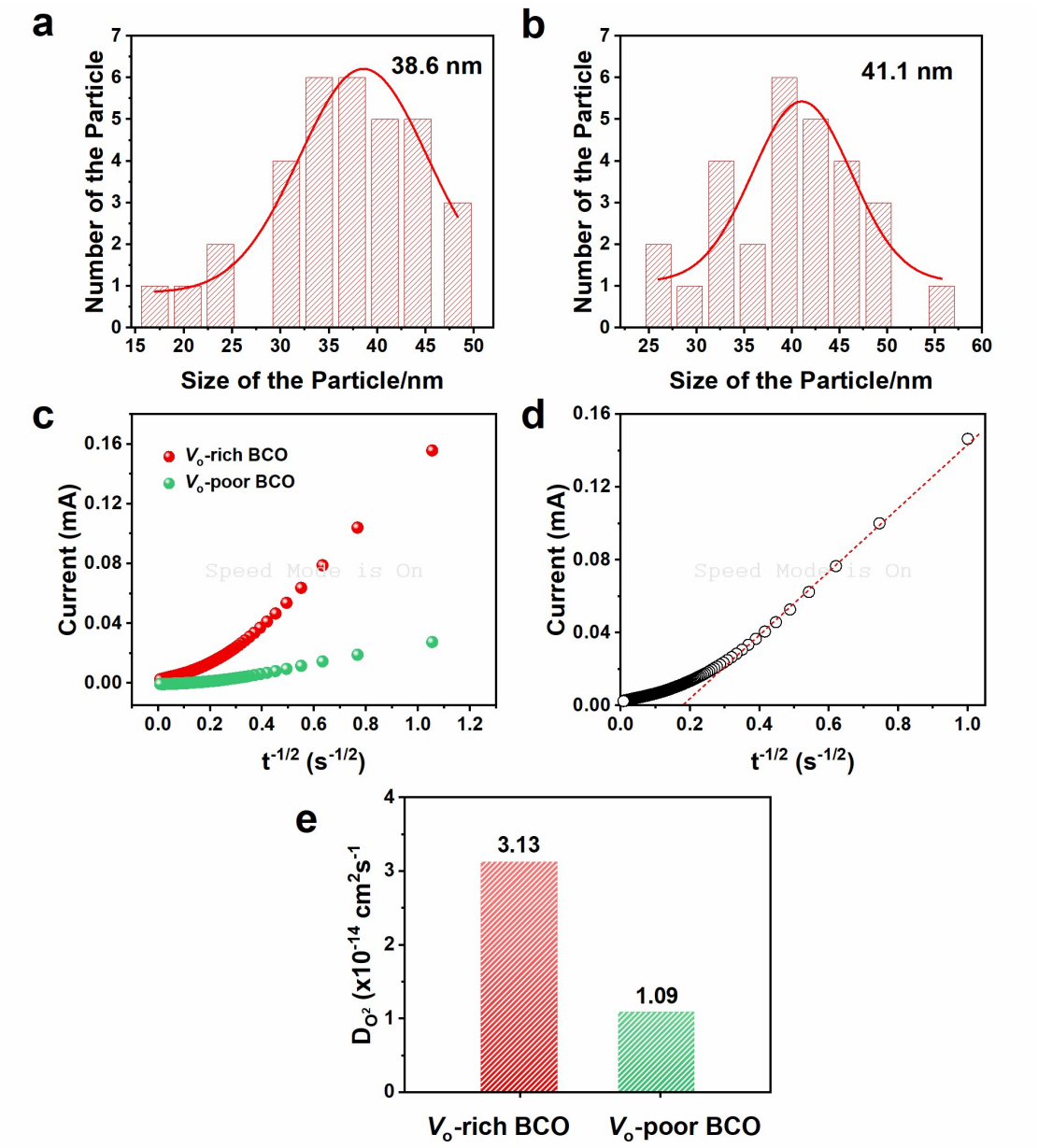

Figure S13. Chronoamperometric oxygen diffusion rate measurements. Sizes of the particle measured from TEM images for a) V_o-rich BCO and b) V_o-poor BCO. (c) Current vs. $t^{-1/2}$ for BCO. (d) Current vs. $t^{-1/2}$ for V_o-rich BCO. e) Oxygen diffusion rates measured at 25 ℃ chronoamperometrically. The diffusion rate can be measured from the intersection of the linear portion of the current vs. $t^{-1/2}$ with the $t^{-1/2}$ axis. The theory is based on a bounded 3D diffusion model, where the intersection of I vs. $t^{-1/2}$ at $I = 0$ corresponds to $\lambda = a/\sqrt{Dt}$, where λ is a dimensionless shape factor, a is the radius of the

particle, D is the diffusion rate, $t^{-1/2}$ is determined from the intersection with the $t^{-1/2}$ axis. In this case, λ is chosen as 2, which is representative of the the round nanosheet-like particles, average between the values for the sphere (λ=1.77) and the cube (λ=2.26). The radius of the particle was obtained from the size distribution, which was counted by the software based on dozens of particles on the TEM images of Figure S2 and then was calculated by Gaussian fitting.

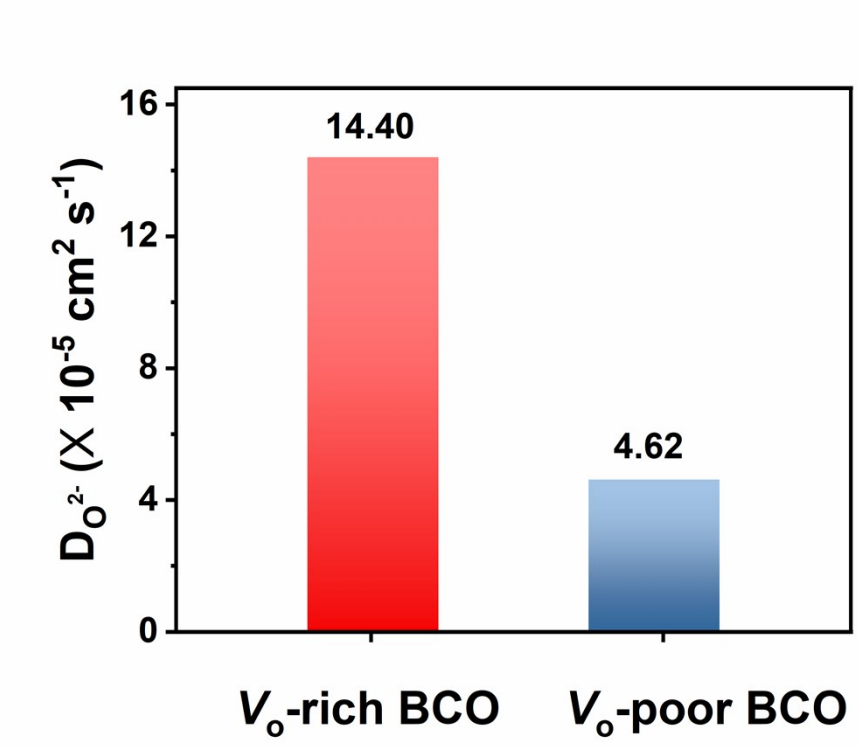

Figure S14. Oxygen diffusion rates measured at 400 ℃ chronoamperometrically. Oxygen diffusion of samples was measured using a four-probe method with a digital multimeter (Keithley, 2001-785D). The samples were firstly pressed into thin slices under 10 *M*Pa, subsequently weresintered at 400 ℃ for 10 h，then were cooled down to 250 ℃ and were maintained for 10 h in a tube furnace under the Air or O_2 atmosphere, respectively. Oxygen incorporation reaction over BCO was characterized using an electronic conductivity relaxation (ECR) method. For these measurements, the oxygen partial pressure N_2 mixture was abruptly changed from 0.21 atm to 1 atm, and the corresponding conductivity change of the BCO sample was recorded as a function of relaxation time.

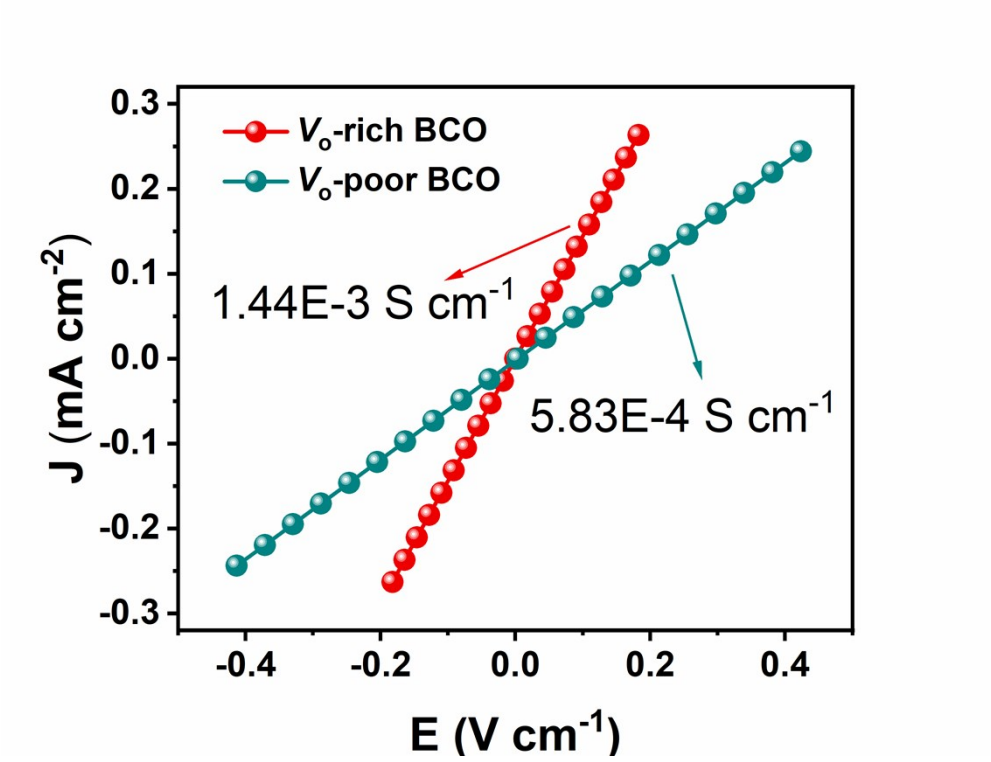

Figure S15. *I–V* curves of V_o-rich and V_o-poor BCO catalysts. For the electrical conductivity measurement, the samples were firstly pressed into thin slices under 10 *M*Pa, the resistances (*R*) were measured using a Keithley model 2000 multimeter instrument. The electrical conductivities (σ) of the samples were calculated via $R=\rho L/S$ and $\sigma=1/\rho$, where ρ, L and S represent the electrical resistivity, length and cross-sectional area of the pressed sample, respectively.

Table S1. Mole ration of Bi and Co in BCO calculated from ICP-AES.

Sample	Mole ratio
V_o-rich BCO	**Bi/Co=0.94:1**
V_o-poor BCO	**Bi/Co=0.98:1**

Table S2. Crystal structure parameters (Å) refined from the measured XRD patterns.

Sample	V_o-rich BCO	V_o-poor BCO
a(Å)	**7.731**	**7.737**
b(Å)	**7.731**	**7.737**
c(Å)	**5.627**	**5.631**
Volume (Å^3)	**336.32**	**337.08**

Table S3. O 1s XPS peak deconvolution results.

Sample	Lattice O^{2-}	O^{2-}/O^-	-OH or O_2	H_2O or CO_3^{2-}
V_o-rich BCO	**56.92%**	**19.84%**	**13.42%**	**9.82%**
V_o-poor BCO	**67.74%**	**10.31%**	**8.42%**	**13.53%**

Table S4. Mole ratio of Bi and Co in BCO calculated from EPMA.

Sample	Bi (%)	Co (%)	O (%)	Bi+Co (%)	δ content
V_o-rich BCO	20.31	21.71	57.98	42.02	0.16
V_o-poor BCO	20.51	20.88	58.61	41.39	0.24

Table S5. Positron lifetime parameters of V_o-rich BCO and V_o-poor BCO.

Sample	τ_1(ps)	τ_2(ps)	τ_3(ns)	I_1(%)	I_2(%)	I_3(%)
V_o-rich BCO	209	363	2.24	31.12	67.02	1.86
V_o-poor BCO	195	364	2.25	33.61	64.37	2.02

Table S6. Comparisons of OER activities of V_o-rich BCO catalyst with other reported electrocatalysts.

Catalysts	Tafel slope (mV/dec)	Overpotential at 10 mA/cm^2 (mV)	electrolyte	Reference
V_o-rich BCO	**43**	**367**	**1.0 M**	**This work**
$LaCoO_3$	69	490	1.0 M	*Nat. Commun.* 2016, **7**, 11510
$SrCoO_{2.85-\delta}F_{0.15}$	60	380	1.0 M	*J. Mater. Chem. A* 2019, **7**, 12538-12546
$Bi_7Co_3Ti_3O_{21}$	87	350	1.0 M	*J. Am. Chem. Soc.* 2019, **141**, 3121-3128
$Sr_3FeCoO_{7-\delta}$	77	426	1.0 M	*J. Mater. Chem. A* 2018, **6**, 14240–14245
$Ba_{0.5}Sr_{0.5}Co_{0.8}Fe_{0.2}O_{3-\delta}$	80	464	1.0 M	*Electrochim. Acta* 2017, **246**, 997–1003
$LaNiO_3$	49	408	1.0 M	*Angew. Chem. Int. Ed.* 2019, **58**, 2316 –2320
$Sr_2Fe_2O_{6-\delta}$	60	480	1.0 M	*Angew. Chem. Int. Ed.* 2019, **58**, 2060
$SrNb_{0.1}Co_{0.7}Fe_{0.3}O_{3-\delta}$	83	420	1.0 M	*Angew. Chem. Int. Ed.* 2015, **54**, 3897 –3901
$La_{0.6}Sr_{0.4}Fe_{0.8}Co_{0.2}O_3$	80	464	1.0 M	*J. Electroanal. Chem.* 2018, **808**, 412–419
$Bi_5CoTi_3O_{15}$&$BiCoO_3$	44	320	1.0 M	*Nat. Commun.* 2019, **10**, 1409
$PrBa_{0.5}Sr_{0.5}Co_{1.5}Fe_{0.5}O_{5+\delta}$	58	313	1.0 M	*Adv. Funct. Mater.* 2019, **29**, 1901783
F substituded $Ba_{0.5}Sr_{0.5}Co_{0.8}Fe_{0.2}O_{3-\delta}$	102.65	280	1.0 M	*Appl. Catal. B Environ.* 2019, **256**, 117817
$Sr_2Fe_2O_{6-\delta}$	60	480	0.1 M	*Angew. Chem. Int. Ed.* 2019, **58**, 2060

$Sr_2Fe_{0.8}Co_{0.2}Mo_{0.6}Co_{0.4}O_{6-\delta}$	60	345	0.1 M	*ChemSusChem.* 2019, **12**, 5111
$Ba_4Sr_4(Co_{0.8}Fe_{0.2})_4O_{15}$	47	340	0.1 M	*Adv. Mater.* 2020, **32**,1905025
$PrBa_{0.5}Sr_{0.5}Co_{1.5}Fe_{0.5}O_{5+\delta}$	52	358	0.1 M	*Nat. Commun.* 2017, **8**, 14586
$SmBa_{0.5}Sr_{0.5}Co_2O_{6-\delta}$	46	370	0.1 M	*J. Mater. Chem. A* 2018, **6**, 4948
$CaCoO_3$	38	260	0.1 M	*Sci. Adv.* 2019, **5**, eaav6262
$SrCoO_{2.7}$	67	417	0.1 M	*Nat. Commun.* 2018, **9**, 3150
$Pr_{0.5}Ba_{0.3}Ca_{0.2}CoO_{3-\delta}$	73	440	0.1 M	*Chem. Commun.* 2017, **53**, 5132
$Sr(Co_{0.8}Fe_{0.2})_{0.95}P_{0.05}O_{3-\delta}$	82.8	400	0.1 M	*ChemNanoMat.* 2019, **5**, 352

Reference

1 S. Zhou, X. Miao, X. Zhao, C. Ma, Y. Qiu, Z. Hu, J. Zhao, L. Shi, J. Zeng, Engineering Electrocatalytic Aactivity in Nanosized Perovskite Cobaltite through Surface Spin-State Transition, *Nat. Commun.*, 2016, **7**, 11510.